PNAS RESEARCH ARTICLE | IMMUNOLOGY AND INFLAMMATION OPEN ACCESS

CryoEM structure of an MHC-I/TAPBPR peptide-bound intermediate reveals the mechanism of antigen proofreading

Yi Sun[a,b], Ruth A. Pumroy[c,1], Leena Mallik[a,b,1], Apala Chaudhuri[a,b], Chloe Wang[c,d], Daniel Hwang[a,b], Julia N. Danon[b], Kimia Dasteh Goli[b], Vera Y. Moiseenkova-Bell[a,c], and Nikolaos G. Sgourakis[a,b,2]

Affiliations are included on p. 9.

Edited by Peter Cresswell, Yale University, New Haven, CT; received August 21, 2024; accepted December 5, 2024

Class I major histocompatibility complex (MHC-I) proteins play a pivotal role in adaptive immunity by displaying epitopic peptides to CD8+ T cells. The chaperones tapasin and TAPBPR promote the selection of immunogenic antigens from a large pool of intracellular peptides. Interactions of chaperoned MHC-I molecules with incoming peptides are transient in nature, and as a result, the precise antigen proofreading mechanism remains elusive. Here, we leverage a high-fidelity TAPBPR variant and conformationally stabilized MHC-I, to determine the solution structure of the human antigen editing complex bound to a peptide decoy by cryogenic electron microscopy (cryo-EM) at an average resolution of 3.0 Å. Antigen proofreading is mediated by transient interactions formed between the nascent peptide binding groove with the P2/P3 peptide anchors, where conserved MHC-I residues stabilize incoming peptides through backbone-focused contacts. Finally, using our high-fidelity chaperone, we demonstrate robust peptide exchange on the cell surface across multiple clinically relevant human MHC-I allomorphs. Our work has important ramifications for understanding the selection of immunogenic epitopes for T cell screening and vaccine design applications.

MHC-I | molecular chaperone | NMR | cryoEM | antigen repertoire

Significance

Major histocompatibility complex (MHC-I) proteins select repertoires of epitopic peptides to display on the cell surface for T cell surveillance, against a vast background of possible decoys. However, the molecular mechanism of this selection, or proofreading, process has remained unclear. Here, we capture a structural snapshot of an MHC-I molecule caught in the act of scrutinizing a potential peptide antigen under the guidance of its molecular chaperone, TAPBPR. The structure shows how conserved MHC-I residues capture the peptide backbone, to enable rapid screening of peptide decoys. TAPBPR facilitates peptide selection by stabilizing this intermediate state rather than directly competing with peptides. These findings advance our understanding of immunogenic epitope selection, with implications for vaccine development and T cell–based therapies.

Class I major histocompatibility complex (MHC-I) proteins display the intracellular proteome onto the cell surface for immunosurveillance by sampling a large pool of peptide fragments (1–3). Optimal high-affinity-peptide-loaded MHC-I (pMHC-I) molecules are recognized by T cell receptors and natural killer receptors, triggering downstream cellular activation and clonal expansion and resulting in the clearance of infected, or aberrant cells (4–6). While the immunogenic peptide repertoires of the Class I Human Leukocyte Antigen (HLA, human MHC-I) proteins are defined by their extremely polymorphic grooves (7–9), selection and optimization of the repertoires in the cellular pathway are mediated by two dedicated molecular chaperones, tapasin (10–13) and TAP binding protein-related (TAPBPR) (14, 15). TAPBPR is a homolog of tapasin that is not part of the peptide loading complex. These chaperones serve as an essential quality control checkpoint for pMHC-I molecules, optimizing the peptide cargo en route to the cell surface (16, 17). Polymorphic residues at the MHC-I groove A-F "pockets" and at the direct interaction surfaces confer a wide range of dependence on chaperones for peptide loading and cell surface expression across various HLA allotypes, with important ramifications for viral control among different individuals (18–22). In addition, chaperones have recently emerged as key components for the presentation of metabolite ligands on MHC-related 1 (MR1) molecules (23–25), and have provided powerful tools for in vitro applications, including the generation of pMHC-I libraries encompassing different peptide specificities or the loading of antigens on cells independently of the endogenous processing pathway (19, 26–28).

Two independently solved crystal structures of mouse MHC-I bound to human TAPBPR (29, 30), together with studies of TAPBPR and tapasin in complex with human MHC-I and MR1 molecules by X-ray crystallography, NMR spectroscopy, and cryogenic electron microscopy (cryo-EM) (23, 31–36) have provided key insights into the chaperoning mechanism. Empty MHC-I adopts an open, peptide-receptive conformation where the short $\alpha_{2\text{-}1}$ helix shifted outward by 3 Å to induce a widened peptide binding groove (29, 30). Based on these structures obtained for the empty, resting state of the complex, it has been proposed that the binding of high-affinity peptides triggers the closure of the MHC-I groove, which allosterically promotes the release of pMHC-I from the chaperone (29, 30, 32). A range of biophysical and biochemical studies have also demonstrated that the affinity of TAPBPR for MHC-I is negatively correlated with peptide occupancy (19, 32, 37, 38). TAPBPR preferentially interacts with nascent empty or suboptimal peptide-loaded

Competing interest statement: N.G.S. is listed as an inventor in a patent application related to this work.

This article is a PNAS Direct Submission.

[1]R.A.P. and L.M. contributed equally to this work.

[2]To whom correspondence may be addressed. Email: nikolaos.sgourakis@pennmedicine.upenn.edu.

This article contains supporting information online at https://www.pnas.org/lookup/suppl/doi:10.1073/pnas.2416992122/-/DCSupplemental.

Published January 9, 2025.

MHC-I molecules, exchanging low- for high-affinity peptides (22). The precise molecular mechanism of MHC-I antigen selection by TAPBPR remains enigmatic (39, 40) due to the transient nature of the peptide/MHC-I/TAPBPR complex, resulting in no structural visualization and precluding a detailed understanding of how TAPBPR edits the peptide repertoire.

To examine the editing function of TAPBPR and capture the biologically relevant peptide-bound state of its MHC-I complex, we have leveraged protein engineering to enhance the stability of MHC-I molecules that are loaded with suboptimal peptides (41), as well as deep scanning mutagenesis of MHC-I binding surfaces on TAPBPR (19). Here, we characterize a high-fidelity chaperone, named TAPBPR^{HiFi}, which shows enhanced binding to peptide-loaded MHC-I molecules and peptide exchange function in vitro. We determine the cryoEM structure of TAPBPR^{HiFi}/HLA-A*02:01/β_2m loaded with a heptameric peptide decoy, revealing a key intermediate of the peptide exchange process. We find that the transient proofreading complex utilizes 1) conserved groove residues to capture the backbone of incoming peptides in a native-like conformation, 2) properly conformed hydrophobic A-, B-, and D-pockets to dock the peptide P2 and P3 anchors, and 3) a conformationally heterogenous F-pocket that folds upon binding to high-affinity peptides, allosterically triggering the dissociation of TAPBPR. Finally, we show that TAPBPR^{HiFi} significantly enhances peptide exchange across multiple HLA-A allotypes expressed on a cellular membrane to promote antigen loading independently of the endogenous pathway, which involves tapasin and the peptide-loading complex. These results have important applications in screening for and eliciting T cell responses in various experimental and therapeutic settings. Taken together, our combined structural, biochemical, and functional studies provide a complete mechanism of MHC-I antigen proofreading and peptide repertoire selection.

Results

Enhanced Editing of MHC-I Antigens Using an Engineered Molecular Chaperone. While contradictory peptide unloading/levering (30, 42, 43) or trapping (38) mechanisms have been proposed involving the G24-R36 loop of TAPBPR, whether the loop actively participates in cargo editing of the peptide-loaded MHC-I molecules remains unclear (39). We sought to resolve this controversy and identify TAPBPR regions that promote interactions with peptide-loaded molecules for antigen editing. Toward this, we used either wildtype TAPBPR, TAPBPR^{WT}, or our engineered version high-fidelity TAPBPR^{HiFi}, containing 3 mutations S104F, K211L, and R270Q outside the loop region (19), to directly measure binding to a high-affinity peptide TAX9 loaded HLA-A*02:01 by surface plasmon resonance (SPR). Experiments were run in the presence of TAX9 peptide in molar excess to prevent peptide dissociation upon binding to TAPBPR. We also compared different mutants of TAPBPR^{HiFi} and TAPBPR^{WT}, containing partial (A29-S32 deletion, TAPBPR$^{\Delta ALAS}$) or complete loop deletions (G24-R36 deletion, TAPBPR$^{\Delta G24\text{-}R36}$, and TAPBPR$^{HiFi\Delta G24\text{-}R36}$) as well as TAPBPR^{TN6} (E205K, R207E, Q209S, and Q272S), which does not interact with peptide-loaded MHC-I (Fig. 1*A* and *SI Appendix*, Fig. S1) (27, 37, 44). Our results showed that TAX9-loaded HLA-A*02:01 exhibited an enhanced affinity (reduced K_D by one order of magnitude) for TAPBPR^{HiFi}, relative to TAPBPR^{WT} (Fig. 1 *B* and *C* and *SI Appendix*, Fig. S2). Meanwhile, loop deletions exhibited no significant effect for TAPBPR^{HiFi} but an approximately threefold decrease in K_D for TAPBPR^{WT} on binding to peptide-loaded MHC-I (Fig. 1 *B* and *C* and *SI Appendix*, Fig. S2), likely due to the loss of hydrophobic interactions with the rim of the MHC-I α_1 and α_2 helices, in agreement with our previous solution mapping studies (38). These observations demonstrate that, by enhancing its interactions with MHC-I surfaces, TAPBPR^{HiFi} improves the recognition of peptide-loaded MHC-I molecules and tolerates loop deletions, compared to the wild type.

We hypothesized that enhanced TAPBPR binding to peptide-loaded MHC-I molecules should correlate with a promotion of peptide dissociation in vitro. We then applied a fluorescence polarization (FP) assay employing HLA-A*02:01 refolded with a TAMRA-labeled TAX9 peptide to directly assess peptide unloading from the MHC-I (41). We found that TAPBPR^{WT} and its loop deletion mutant, TAPBPR$^{\Delta G24\text{-}R36}$, demonstrated a similarly low level of peptide unloading, relative to the negative controls (Fig. 1 *D* and *E*). Notably, both TAPBPR^{HiFi} and TAPBPR$^{HiFi\Delta G24\text{-}R36}$ significantly improved peptide unloading function (Fig. 1 *D* and *E*). However, introducing the G24-R36 loop deletion on either TAPBPR^{WT} or TAPBPR^{HiFi} had no functional impact on MHC-I peptide editing in vitro (Fig. 1*E*). Taken together, our results confirm that, while the G24-R36 loop plays a role in maintaining TAPBPR's structural integrity for pMHC-I recognition, surfaces outside the loop are essential for promoting interactions with peptide-loaded MHC-I and enhancing the editing capability of TAPBPR (19).

To determine the MHC-I allelic interaction landscape of TAPBPR^{HiFi}, we applied a SAB assay encompassing 97 common HLA allotypes (19, 46, 47). We measured the phycoerythrin (PE) mean fluorescent intensity (MFI) of SABs upon incubation with TAPBPR^{HiFi} or TAPBPR^{WT} PE-tetramers. The levels of nonspecific background binding to HLAs are controled by the corresponding TAPBPR PE-tetramer staining of SABs that are preincubated with W6/32, a pan-allelic HLA monoclonal antibody, which blocks the TAPBPR interaction surface on MHC-I, and further compared to the staining of TAPBPR^{TN6} PE-tetramer (*SI Appendix*, Fig. S3 *A* and *B*). Analysis of MFI ratios for TAPBPR^{HiFi} revealed enhanced interactions with multiple HLA allotypes, including HLA-A*02:01, A*02:03, A*02:06, A*69:01, A*68:01, A*23:01, A*24:02, and A*24:03, relative to TAPBPR^{WT} (Fig. 1*F* and *SI Appendix*, Fig. S3*C* and *D*). Together, these results demonstrate that a broad range of HLA-A* allotypes are prone to enhanced recognition by TAPBPR^{HiFi}, which can further promote peptide editing, indicating its potential as an exogenous peptide exchange catalyst (27).

Solution Mapping of TAPBPR^{HiFi} Interactions with Peptide-Loaded MHC-I. We, therefore, ask how TAPBPR^{HiFi} acts on properly conformed, peptide-loaded MHC-I compared to TAPBPR^{WT} in a solution environment to achieve enhanced binding affinity and editing function. We used methyl-based NMR spectroscopy to map TAPBPR^{HiFi} interactions with high-affinity peptide TAX9-loaded HLA-A*02:01, as established previously (22, 32, 48). By titrating unlabeled TAPBPR^{HiFi} on isotopically methyl-labeled (AILV) HLA-A*02:01 using established methods (22, 32, 38), 42 out of 96 resonances undergo chemical shift changes in the slow exchange regime, which is similar to the changes observed upon binding to TAPBPR^{WT} (Fig. 2*A* and *SI Appendix*, Fig. S4*A*). We observed a complete shift in the population to a chaperone-bound form for nearly all resonances at a three-fold molar excess of TAPBPR^{HiFi} (Fig. 2*B* and *SI Appendix*, Fig. S4 *A* and *B*), indicating the presence of a high-affinity complex. Analysis of methyl $^{13}C/^{1}H$ chemical shift deviations (CSDs) captures the residues that experience significant conformational changes (≥ 0.5SD) based on the difference in the local magnetic environment (Fig. 2*C*). Comparing the CSDs of TAX9-loaded HLA-A*02:01 induced by binding to TAPBPR^{HiFi} relative to

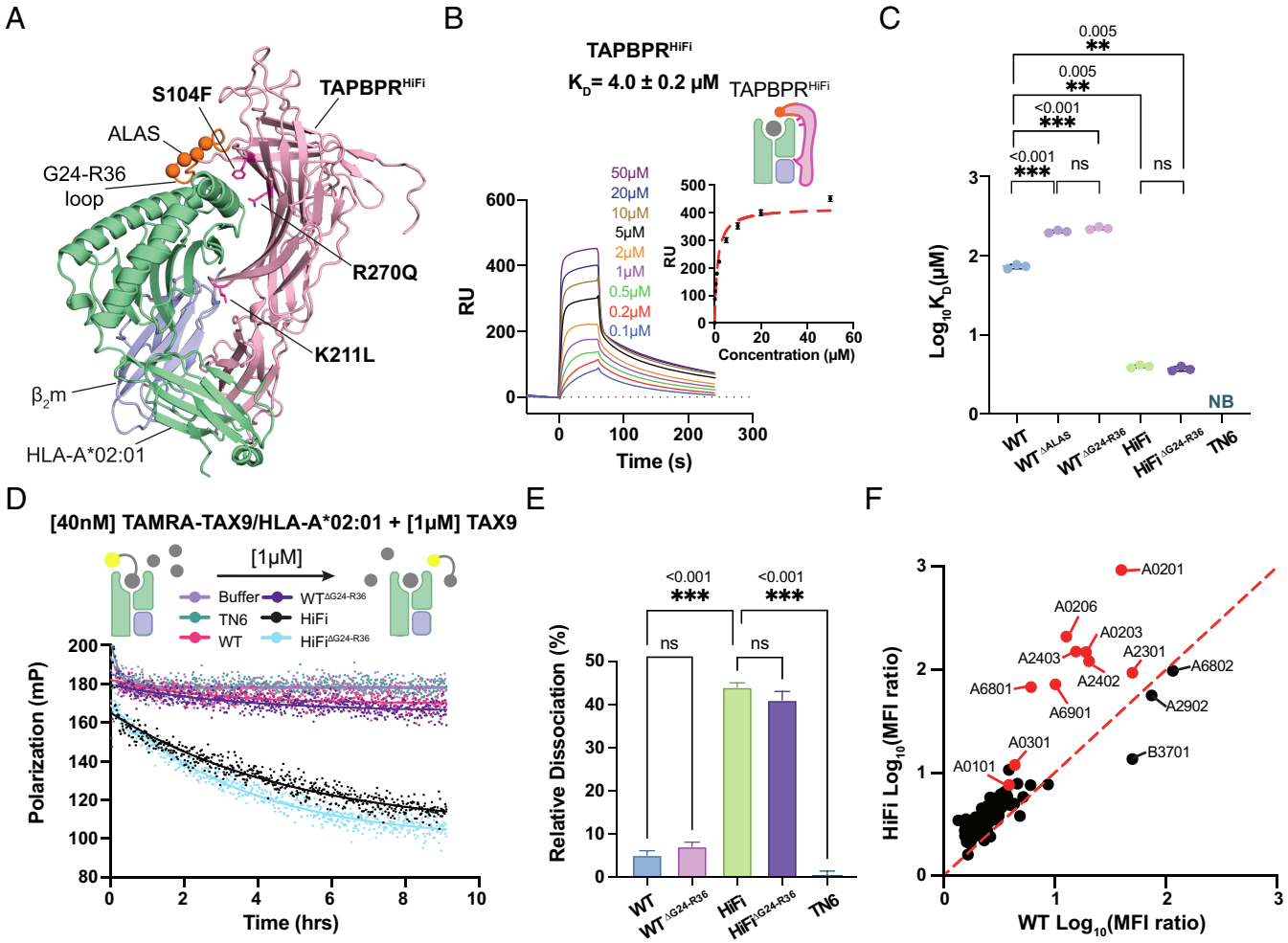

Fig. 1. A high-fidelity TAPBPR variant TAPBPR^{HiFi} enhances peptide editing on peptide-loaded MHC-I. (*A*) Structural model of TAPBPR^{HiFi} in complex with peptide-free HLA-A*02:01/β_2m generated using RosettaCM (45). The G24-R36 loop is colored orange, and the A29-S32 loop segment is shown as spheres. The sidechains of mutations S104F, K211L, and R270Q are shown as magenta sticks. (*B*) Representative SPR sensorgram of graded concentrations of TAPBPR^{HiFi} flown over a streptavidin chip coupled with TAX9/HLA-A*02:01 in excess TAX9 peptide. (*C*) Log-scale comparison of K_D values between TAX9/HLA-A*02:01 and TAPBPR. Results of three independent experiments (mean ± SD) are shown as scatter plots. (*D*) Peptide dissociation kinetics of fluorophore-labeled TAMRA-TAX9-(TAMRA-KLFGYPVYV)-peptide-loaded HLA-A*02:01 in the presence of excess unlabeled TAX9 peptide with buffer (light purple), TAPBPR^{TN6} (green), TAPBPR^{WT} (magenta), TAPBPR$^{\Delta G24\text{-}R36}$ (purple), TAPBPR^{HiFi} (light blue), and TAPBPR$^{HiFi\Delta G24\text{-}R36}$ (black). Data are means for n = 3 independent experiments. (*E*) Relative peptide dissociation of TAMRA-TAX9 from HLA-A*02:01 by TAPBPR relative to no TAPBPR. The relative dissociation was calculated using the equation $\%relativedissociation = \frac{Plateau^{bufferonly} - Plateau^{chaperone}}{Plateau^{buffer\ only}}$, and the plateau for each dissociation was individually extracted by fitting one phase decay. Error bars (SD) were propagated from three independent experiments. (*F*) Comparison of binding profiles for TAPBPR^{WT} and TAPBPR^{HiFi} against a panel of 97 common HLA allotypes using single antigen beads (SABs). Two-sample unequal variance Student's *t*-test was performed, $P > 0.12$ (not significant, ns), $P < 0.033$(*), $P < 0.002$(**), and $P < 0.001$(***). *SI Appendix*, Figs. S1–S3.

TAPBPR^{WT} results in a Pearson correlation coefficient of 0.93 (Fig. 2*D*), suggesting that TAX9/HLA*02:01 shifts to a similar conformational state when bound to TAPBPR^{HiFi} or TAPBPR^{WT}. Taken together, TAPBPR^{HiFi} docks on MHC-I using an overall similar binding mode, in comparison to our previous solution mapping of interactions between TAX9/HLA-A*02:01 with wildtype TAPBPR (22, 38).

Our NMR data showed that residues, such as A117, A125, and L126, located near the TAPBPR interface demonstrated significant CSDs (Fig. 2*E*). Multiple residues like I23 and V34 that are located more than 10 Å away from the interface or within the peptide binding groove also exhibited significant CSDs (Fig. 2*E*), indicating allosteric, long-range effects on pMHC-I by TAPBPR^{HiFi}, consistently with previous studies (22, 32). Next, we used a line shape analysis of our 2D methyl HSQC spectra to determine the affinity between TAPBPR^{HiFi} and high-affinity peptide-loaded HLA-A*02:01. Consistent with our previous SPR measurements, TAPBPR^{HiFi} demonstrated a low micromolar-range affinity (K_D = 13.9 μM) (*SI Appendix*, Table S1) when fitting the resonances that undergo conformational changes to a two-state binding model (*SI Appendix*, Fig. S4*C*). Together, these observations indicated that pMHC-I molecules experience similar structural changes upon binding to TAPBPR^{HiFi} or TAPBPR^{WT}. This motivated us to use TAPBPR^{HiFi} to stabilize MHC-I in its peptide editing state, and visualize the MHC-I/TAPBPR proofreading complex.

CryoEM Structure of the MHC-I/TAPBPR Complex Bound to a Peptide Decoy. We reasoned that the enhanced affinity of TAPBPR^{HiFi} for pMHC-I could capture transient, unstable peptide-editing complexes. To define the structural basis of peptide antigen proofreading and selection by TAPBPR, we leveraged our enhanced peptide editor, TAPBPR^{HiFi}, to isolate a tertiary complex prepared with open HLA-A*02:01 (G120C) refolded with β_2m (H31C) (41) and a photocleavable peptide (KILGFVFJV, J = 3-amino-3-(2-nitrophenyl)-propionic acid) used as a conditional ligand (49, 50). Upon UV irradiation, we purified soluble TAPBPR^{HiFi} in complexes

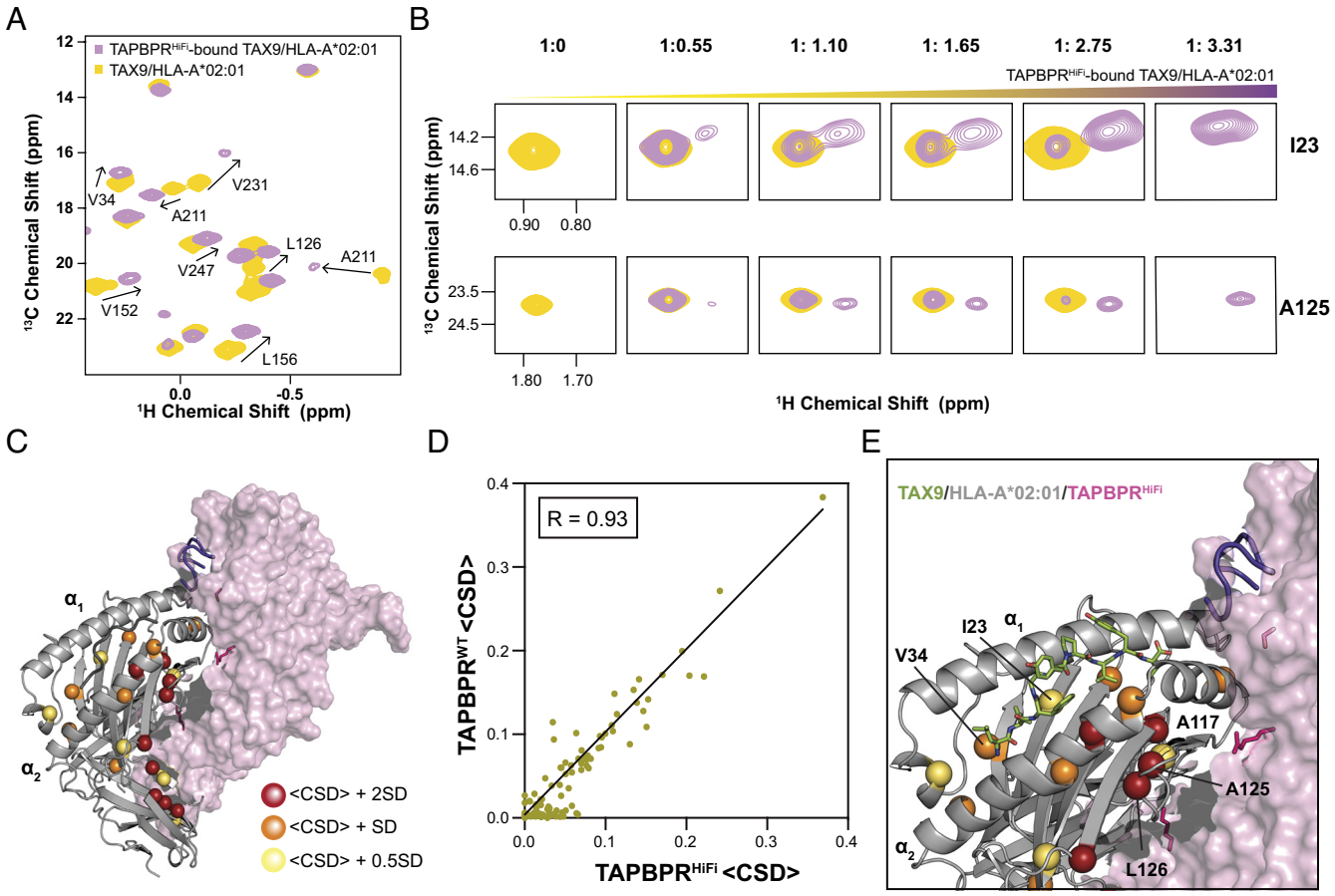

Fig. 2. TAPBPR^{HiFi} uses a conserved docking mode to recognize peptide-loaded HLA-A*02:01 in solution. (*A*) A representative region of the 2D ^{1}H-^{13}C HMQC spectral overlay of selectively ^{13}C/^{1}H AILV methyl-labeled HLA-A*02:01/TAX9/β_2m (at the heavy chain) on a ^{12}C/^{2}H background (yellow) and with a threefold molar excess of TAPBPR^{HiFi} at natural isotopic abundance (purple). (*B*) Selected NMR resonances (corresponding to the methyl sidechains of I23 and A125) undergoing conformational exchange between the free and TAPBPR^{HiFi}-bound states. The HLA-A*02:01: TAPBPR^{HiFi} molar ratios for the different titration points were 1: 0, 1: 0.55, 1: 1.10, 1: 1.65, 1: 2.75, and 1: 3.31. (*C*) Methyl groups of residues undergoing significant CSD upon binding of TAPBPR^{HiFi} are mapped onto the structure of the HLA-A*02:01 (gray)/TAPBPR^{HiFi} (pink) complex. The structure is a RosettaCM (45) homology model obtained using the H2-D^{d}/TAPBPR crystal structure as a template (PDB ID: 5WER). CSDs are plotted using a heat-map scale shown on the *Right*. (*D*) Correlation plot of CSDs observed for the titration of HLA-A*02:01 with TAPBPR^{WT21,41} versus TAPBPR^{HiFi}. The Pearson correlation coefficient (r) is shown on the plot (*P* value < 0.0001). (*E*) Close-up of the peptide-binding groove with the TAX9 peptide (shown as green sticks). Select residues distributed throughout the MHC-I groove and their methyl CSDs are labeled. The three mutation sites on TAPBPR^{HiFi} are denoted with pink sticks, and the approximate location of the unstructured G24-R36 loop region is highlighted in dark purple. *SI Appendix*, Fig. S4.

with open HLA-A*02:01/β_2m by size exclusion chromatography (SEC) (Fig. 3*A*). Further analysis by LC–MS revealed that a 7-mer peptide decoy (KILGFVF) was captured within the TAPBPR/MHC-I complex (Fig. 3*B* and *SI Appendix*, Fig. S5). We solved the structure of this purified 90 kDa complex using cryoEM (*SI Appendix*, Table S2). Briefly, purified peptide-loaded open HLA-A*02:01/TAPBPR^{HiFi} was used to screen grids, and more than 5,000 micrographs were collected (*SI Appendix*, Fig. S6). This dataset revealed a fully assembled MHC-I/TAPBPR complex with a well-defined peptide binding groove, though with some heterogeneity in peptide occupancy. We sorted the dataset to obtain a set of particles with the best occupancy of the first residues of our peptide decoy, obtaining a structure at an overall resolution of 3.0 Å (*SI Appendix*, Figs. S7 and S8).

Inspection of our structural model built into well-defined regions of the electron density reveals key chaperoning interactions between peptide-loaded MHC-I and TAPBPR (Fig. 3*C*). In agreement with previous studies (29, 30), we observe that the N-terminal immunoglobulin V (IgV)–like domain of TAPBPR^{HiFi} cradles the pMHC-I peptide binding groove, while the C-terminal IgC domain nestles between the pMHC-I α_3 and β_2m domains to create a pseudo-3-fold symmetric arrangement (Fig. 3*C*). The overall binding mode of TAPBPR is polarized toward the α_2 helix of the pMHC-I peptide binding groove (Fig. 3*C*), consistent with the crystal structures of empty mouse MHC-I/TAPBPR complexes (29, 30) as well as extensive mapping of human MHC-I/TAPBPR interactions by NMR, hydrogen–deuterium exchange, and deep scanning mutagenesis (19, 22, 32). Interactions between TAPBPR and the groove of pMHC-I are mediated through G212 and T259, forming polar contacts with Q115, K121, and D122 on strands β7 and β8, located under the peptide binding groove (Fig. 3*D*). We also observe interactions between TAPBPR residues Q336 and F331 with L231 from α_3 and residues I92-K94 from β_2m, while D309 of TAPBPR forms a hydrogen bond with the T4 sidechain from β_2m (Fig. 3*E*). These results are in good overall agreement with the CSDs obtained from our solution NMR mapping of the complex (Fig. 2). In summary, a triad of domain interactions between β_2m, pMHC-I α_3, and C terminal TAPBPR mediate stable docking, and allow TAPBPR to stabilize the floor and $\alpha_{2\text{-}1}$ helix of the peptide binding groove of peptide-loaded MHC-I molecules, setting the stage for peptide editing to proceed.

Peptide-Loaded MHC-I/TAPBPR Complex Reveals Unexpected Structural Alterations. To understand the molecular mechanism of peptide editing and conformational changes induced by peptide binding to the MHC-I/TAPBPR proofreading complex, we performed a structural comparison of our partially loaded KILGFVF/HLA-A*02:01/TAPBPR cryoEM structure relative to the fully loaded HLA-A*02:01/GILGFVFTL X-ray structure

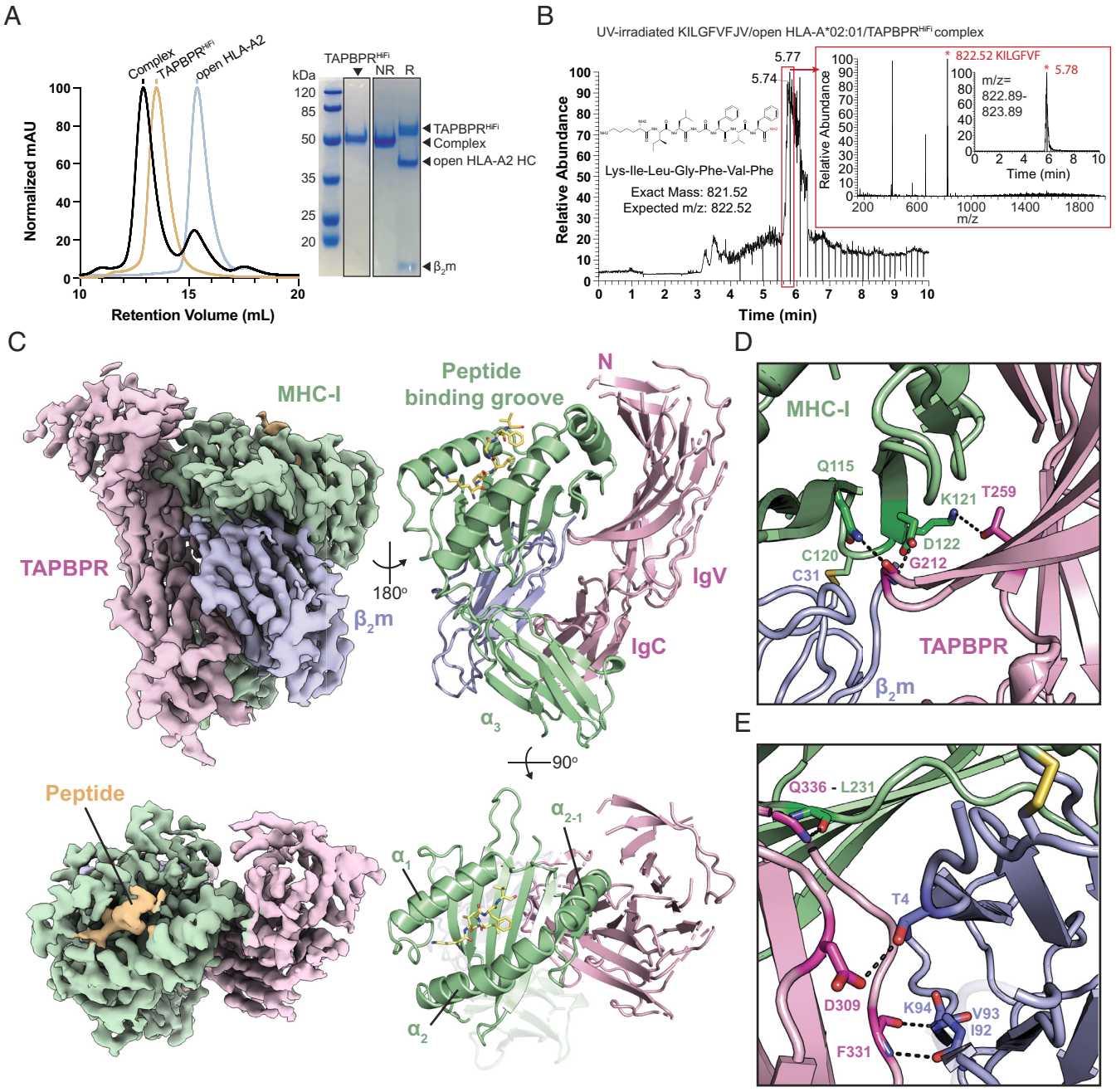

Fig. 3. Isolation and cryoEM structure of an MHC-I/TAPBPR complex bound to a peptide decoy. (*A*) SEC purification of a recombinant open HLA-A*02:01/TAPBPR^{HiFi} complex prepared by UV-irradiation of KILGFVFJV/HLA-A*02:01 preincubated with TAPBPR^{HiFi} at 1:1.3 molar ratio. J = 3-amino-3-(2-nitrophenyl)-propionic acid. Sodium dodecyl sulfate/polyacrylamide gel electrophoresis analysis confirms the identity of the TAPBPR^{HiFi}/open HLA-A*02:01 complex peak under nonreducing (NR) or reducing (R) conditions. The bands of TAPBPR^{HiFi}, open HLA-A*02:01 heavy chain (HC), and β_2m, as well as the positions of molecular weight standards, are indicated. (*B*) LC/MS analysis of the purified complex in Fig. 3*A* showing the presence of captured peptide decoy KILGFVF (observed and expected mass-to-charge ratios are 822.52 and 822.50 m/z, respectively). (*C*) Reconstructed cryoEM density and refined structural model of the tertiary complex, with TAPBPR^{HiFi} shown in light pink, open HLA-A*02:01 heavy chain in pale green, β_2m in light blue, and peptide in wheat, as indicated. (*D*) Zoom in on the interactions between the TAPBPR^{HiFi} hairpin and the floor of the MHC-I peptide binding groove. (*E*) Zoom in on the interactions among TAPBPR^{HiFi} IgC domain residues, MHC-I α_3, and β_2m, highlighting the sidechain interaction between TAPBPR^{HiFi}, MHC-I, and β_2m. *SI Appendix*, Figs. S5–S8.

(Fig. 4*A* and Movie S1) (51). We find that the $\alpha_{2\text{-}1}$ helix, comprising residues E148-H151, adopts a conformation that is widened by approximately 3 Å in the TAPBPR-bound complex relative to the fully loaded pMHC-I structure (measured at the Cα atom of A150, Fig. 4*B*), in line with the observations made on the basis of empty MHC-I/TAPBPR complexes (29, 30). Notably, in contrast to the previous empty TAPBPR/MHC-I crystal structures as well as the fully loaded pMHC-I structure, our cryoEM structure reveals a significant alteration of the α_1 helix and adjacent loop (residues S71-G91) (Fig. 4*B* and Movie S2), where a lack of clear electron density indicates the presence of conformational heterogeneity impacting the F-pocket of the peptide-binding groove (*SI Appendix*, Fig. S8). This finding reflects the dynamic transitions of the F-pocket between peptide-deficient and peptide-bound states in a solution environment (Movie S2), in agreement with our previous NMR studies of MHC-I/TAPBPR complexes (32).

Compared to the original influenza epitope GILGFVFTL, the heptamer peptide decoy (KILGFVF) within the TAPBPR editing complex exhibits a native-like backbone conformation and sidechain rotamer placement (Fig. 4 *A* and *C* and Movie S1). Despite the

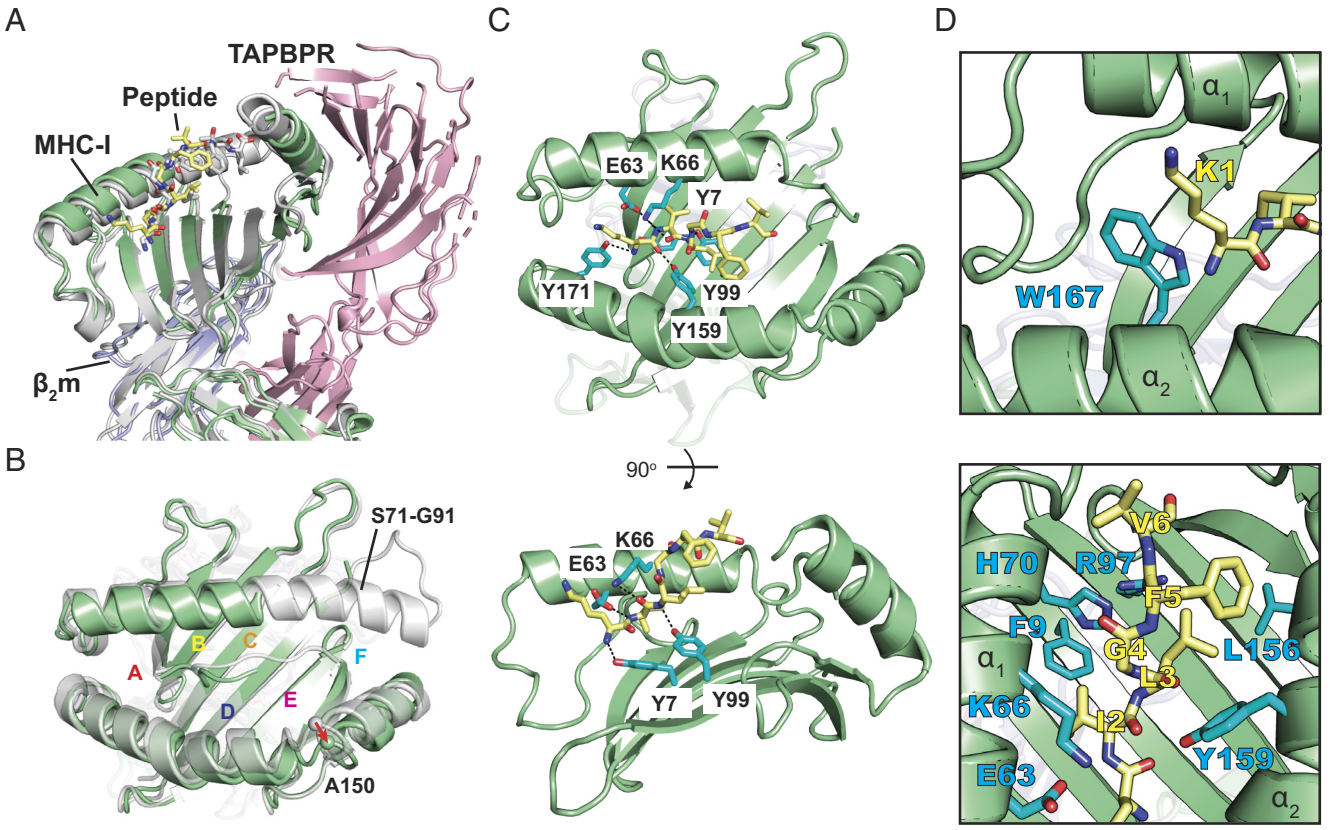

Fig. 4. Structural changes between free and chaperoned, peptide-bound HLA-A*02:01. (*A*) Overview of the molecular complex between TAPBPR^{HiFi}/HLA-A*02:01/β_2m with a peptide decoy [PDB ID 9C96 (52), EMDB ID EMD-45360 (53)], shown as light pink, pale green, light blue cartoons, and yellow sticks, respectively, overlaying with peptide-loaded (GILGFVFTL) HLA-A*02:01 (PDB ID 2VLL) shown in gray. The MHC-I α_2 helix has been partially removed for peptide visualization. (*B*) Structural superposition of chaperone-free peptide-loaded HLA-A*02:01 (PDB ID 2VLL) onto the cryoEM structure of chaperoned KILGFVF/HLA-A*02:01 [PDB ID 9C96 (52), EMDB ID EMD-45360 (53)] showing well-resolved density for peptide residues 1-6, and a lack of cryoEM density for residues S71-G91 of HLA-A*02:01. MHC-I A-, B-, C-, D-, E-, and F-pockets are noted and the spheres are showing A150 Cα. (*C*) Detailed interactions between MHC-I groove residues with the backbone of peptide residues P1-P3, as indicated (*Top* and side views). Hydrogen bonds are indicated by black dashed lines. (*D*) Close-up view of the molecular interactions between the N-terminal peptide hydrophobic sidechain with MHC-I peptide binding groove residues. *SI Appendix*, Fig. S9.

highly polymorphic character of the MHC-I peptide binding groove, a relatively conserved cluster of residues (Y7, E63, K66, Y99, Y159, and Y171) located within the A-, B-, and D-pockets mediate stable docking interactions with the peptide backbone (Fig. 4*C* and *SI Appendix*, Fig. S9 and Movie S1) (54). Additional groove residues, including W167, F9, H70, L156, and Y159, with hydrophobic sidechain anchors the N-terminus of the peptide, particularly at the P2 and P3 positions (Fig. 4*D* and Movie S1). While some amino acid polymorphisms across common HLA allotypes can be observed at positions 63 and 66 (E63 and K66 for HLA-A*02:01), with the exception of I66, all other possible amino acid polymorphisms have the potential to serve as hydrogen bond donors to the carbonyl oxygen of the peptide at P3 (Fig. 4*D*). However, the dynamic character of the S71-G91 region in the editing complex leads to missing interactions between the C-terminus of the peptide with residues D77, Y84, T143, and W147 of the E- and F-pockets (*SI Appendix*, Fig. S9 and Movie S1). It is worth noting that our observed MHC-I structural adaptations are induced by binding to TAPBPR, rather than a loss of the two C-terminal peptide residues in our decoy model. This is highlighted by a structural superposition of our chaperoned pMHC-I relative to a previously determined X-ray structure of HLA-A*02:01 bound to a 4-residue N-terminal peptide fragment (55), which consistently shows a widening of the $\alpha_{2\text{-}1}$ helix at Ala 150, and induced disruption of the structural environment in the MHC-I F-pocket (*SI Appendix*, Fig. S10). This suggests that the inherent flexibility of the F-pocket, in agreement with previous studies (22, 32, 56, 57), can provide an additional filter to select high-affinity interactions with the C-terminus of candidate peptides.

Placing in the context of previous NMR and X-ray studies (22, 29, 30, 32, 38), our cryo-EM structure demonstrates that the initial capture of peptides for proofreading by TAPBPR occurs through native-like interactions with conserved MHC-I residues within the A-, B-, and D-pockets that are properly conformed to receive the peptide. The F-pocket is partially formed in this intermediate state of the complex and folds upon annealing of peptide C-terminus for high-affinity ligands with robust P9 anchors, allosterically shifting the groove inward via $\alpha_{2\text{-}1}$ helix and promoting the dissociation of TAPBPR from the pMHC-I complex (32). These functional and structural results altogether suggest that peptide-loaded MHC-I can form high-affinity, stable proofreading complexes with TAPBPR for antigen selection.

TAPBPR^{HiFi} Enhances Loading of Exogenous Antigens on the Cell Surface. We hypothesized that TAPBPR^{HiFi} could enhance the exchange of peptides on different HLA-A allotypes expressed on a cellular surface. Using a flow cytometry-based method, we assessed the loading of fluorophore-labeled peptides upon incubation with soluble TAPBPR variants, TAPBPR^{HiFi}, TAPBPR^{WT}, and TAPBPR^{TN6}, at different concentrations for monoallelic 722.211 cell lines (58) expressing either HLA-A*02:01, 24:02, 23:01, 03:01, 68:01, 01:01, or 11:01 (Fig. 5*A* and *SI Appendix*, Fig. S11). Consistent with our bead-based binding data, we found

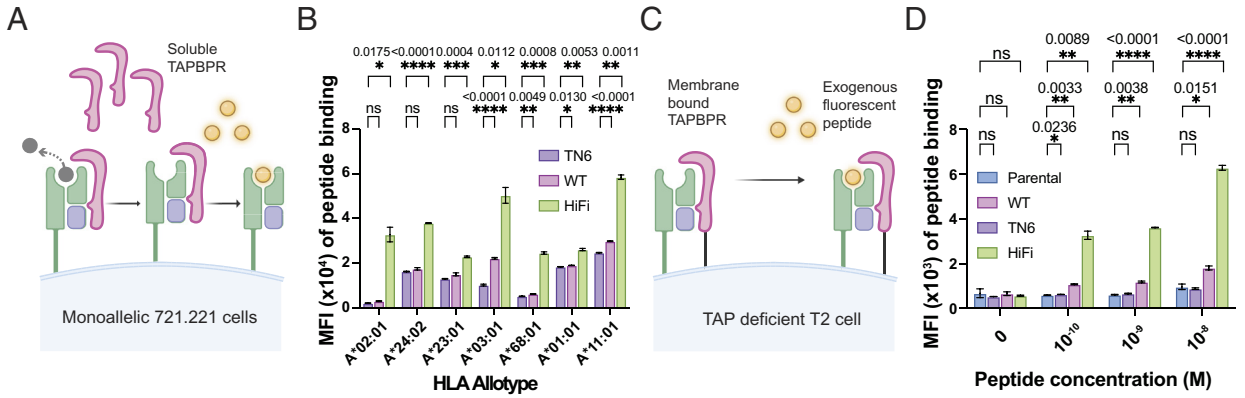

Fig. 5. TAPBPR^{HiFi} enhances peptide loading across common HLA-A* allotypes expressed on a cellular membrane. (*A*) Schematic of peptide exchange for MHC-I expressed on the cell surface by soluble TAPBPR. (*B*) Bar graph summarizing the median fluorescence intensity (MFI) of fluorescent peptide binding for monoallelic HLA-A*02:01, A*24:02, and A*23:01 cell lines with 10 nM fluorescent peptide and 1 μM TAPBPR^{HiFi}, TAPBPR^{WT}, or TAPBPR^{TN6}, and HLA-A*03:01, A*68:01, A*01:01, and A*11:01 cell line in the presence of 10 μM fluorescent peptide and 10 μM TAPBPR^{HiFi}, TAPBPR^{WT}, or TAPBPR^{TN6}, as indicated, from three independent experiments. Two-way ANOVA was performed relative to TAPBPR^{TN6}, $P > 0.0.1234$ (ns), $P < 0.0332$(*), $P < 0.0021$(**), $P < 0.0002$(***), and $P < 0.0001$(****). (*C*) Schematic of peptide exchange for MHC-I expressed on the cell surface by membrane-bound TAPBPR. (*D*) Bar graph summarizing the MFI of fluorescent peptide binding to HLA-A*02:01 expressed T2 cell line with no transduction (parental) or TAPBPR^{HiFi}, TAPBPR^{WT}, or TAPBPR^{TN6}-TM transduction, in the presence of different concentrations of fluorophore-labeled peptide as indicated, from three independent experiments. Two-way ANOVA was performed relative to the parental (no transduction), $P > 0.0.1234$ (ns), $P < 0.0332$(*), $P < 0.0021$(**), $P < 0.0002$(***), and $P < 0.0001$(****). *SI Appendix*, Figs. S11–S13.

that a nanomolar-range concentration of TAPBPR^{HiFi} can readily exchange peptides on membrane-bound HLA-A*02:01, relative to the negative control TAPBPR^{TN6}, whereas TAPBPR^{WT} shows no significant enhancement in exchanging for targeted fluorophore-labeled peptides (Fig. 5*B* and *SI Appendix*, Fig. S12*A*). Similarly, using monoallelic HLA-A*24:02 and HLA-A*23:01 cell lines, we observed that TAPBPR^{HiFi} can promote robust peptide exchange at a concentration that is two orders of magnitude lower than TAPBPR^{WT} (Fig. 5*B* and *SI Appendix*, Fig. S12 *B* and *C*). Despite showing lower levels of binding to MHC-I coated beads in our assay (Fig. 1*F*), TAPBPR^{HiFi} can readily load exogenous peptides on HLA-A*03:01, HLA-A*68:01, HLA-A*01:01, and HLA-A*11:01 (Fig. 5*B* and *SI Appendix*, Fig. S12 *D*–*G*). Generally, we observe that the capability of TAPBPR variants to catalyze peptide exchange on monoallelic cells is correlated to their binding levels on pHLA molecules as measured by our SAB assay (Fig. 1*F*). These results demonstrate that TAPBPR ^{HiFi} can readily load exogenous peptides on multiple HLA-A allotypes via direct interactions on the cell surface.

We next evaluated whether TAPBPR^{HiFi}-TM, a version of TAPBPR containing the TM and cytosolic tail from HLA-G (19, 22) expressed on the cell surface of TAP transporter deficient T2 cells (59, 60) that lack the endogenous antigen processing machinery can directly enhance the loading of exogenous, fluorescently labeled peptides (Fig. 5*C* and *SI Appendix*, Fig. S13*A*). Our results showed that TAPBPR^{HiFi}-TM can significantly enhance the level of peptide loading at low peptide concentrations relative to T2 cells expressing TAPBPR^{TN6} -TM or TAPBPR^{WT}-TM (Fig. 5*D* and *SI Appendix*, Fig. S13 *B* and *C*). We further demonstrate that surface-expressed TAPBPR^{HiFi}-TM increases the expression level of HLA-A*02:01 on the T2 cell surface, as measured by staining with the allele-specific BB7.2 anti-HLA A2 antibody (*SI Appendix*, Fig. S13*D*). HLA-A*02:01 molecules on T2 cells expressing TAPBPR^{HiFi}-TM are receptive to peptide binding at a picomolar-range concentration (Fig. 5*D* and *SI Appendix*, Fig. S13*D*). Taken together, our results demonstrate that our engineered high-fidelity TAPBPR variant TAPBPR^{HiFi} can have a wide range of applications in promoting peptide exchange and participating in antigen selection across different HLA-A* allotypes, directly on the cell surface.

Discussion

The molecular chaperones tapasin and TAPBPR play important roles in stabilizing nascent MHC-I molecules, optimizing the repertoire of bound peptide cargo, and mediating quality control of peptide-loaded molecules, in tandem with other components of the MHC-I antigen processing pathway (1, 2, 61–63). Advances in sample preparation and the use of complementary structural techniques have provided multiple resting-state (empty) MHC-I/chaperone complex structures, which have established the basis of tapasin and TAPBPR recognition of peptide-deficient MHC-I molecules (64, 65). Notwithstanding, the molecular mechanism of peptide editing is enigmatic and highly controversial in the literature (39). In previous work, we used solution NMR methyl probes to study a peptide-bound MHC-I/TAPBPR intermediate and showed that it involves a transient conformational state (approximately 200 millisecond lifetime) (32). A large body of work has established that dynamics at residues distributed throughout the MHC-I peptide binding groove are dampened upon binding of high-affinity peptides, and allosterically coupled to the TAPBPR binding surfaces on the underside and $\alpha_{2\text{-}1}$ helix of the groove to promote chaperone release from the pMHC-I (22, 32, 38). Recent X-ray structures of HLA-B*08:01 bound to 20 mer peptides with protruding N-terminus have provided clues into the peptide-bound intermediate of the loading process (66). Despite these insights, a high-resolution structure of the transient peptide-bound chaperoned MHC-I has been missing due to its transient nature and dynamic complexity, hindering structure determination by X-ray crystallography or cryoEM.

We here leverage recent advances in protein engineering of the individual components, a high-fidelity TAPBPR^{HiFi} variant (19), and an ultrastable, open HLA-A*02:01 molecule (41) prepared using a photocleavable conditional peptide ligand (67), to isolate a TAPBPR/MHC-I intermediate bound to a heptamer peptide decoy. The insights gained from our peptide-loaded MHC-I/TAPBPR cryoEM structure allow us to propose the following mechanism for peptide proofreading on MHC-I (Fig. 6). Empty MHC-I is preferentially recognized and stabilized by TAPBPR in a peptide-receptive, "open" state. Chaperoned MHC-I molecules screen the large peptide pool within the endoplasmic reticulum, via transient peptide/MHC-I/TAPBPR complexes. Meanwhile, TABBPR widens

the peptide binding groove via the $\alpha_{2\text{-}1}$ helix and enhances dynamic movements alongside the α_1 helix and F-pocket. This inherent plasticity of the $\alpha_{2\text{-}1}$ helix has been revealed in previous studies addressing interactions with chaperones by NMR (32, 68), and shown to be important for the sampling of a sparse, open MHC-I state which is recognized with high-affinity by TAPBPR (22). As a result, key peptide-coordinating residues within the E- and F-pockets show a reduced potential for interactions with the peptide C-terminus. Therefore, TAPBPR-bound MHC-I exhibits an overall lower affinity toward incoming peptides, and promotes the dissociation of transiently bound peptide decoys. When chaperoned MHC-I proofreads a high-affinity peptide, it interacts with the N terminal peptide through native-like contacts formed within the A-, B-, and D-pockets. The C-terminus of high-affinity peptides interacts with peptide-coordinating residues in the E- and F- pockets to stabilize and close the peptide binding groove, which allosterically triggers the release of TAPBPR (32). The resulting high-affinity peptide-loaded MHC-I that has been proofread by TAPBPR can traffic to the cell surface for antigen presentation (Fig. 6).

The persistence of class I MHC molecules on the cell surface is determined by their thermodynamic and kinetic stability. Loss of the bound peptide results in destabilization of the complex and disassembly of β_2m, which triggers internalization and endosomal recycling or lysosomal degradation of unfolded molecules via an unknown mechanism (69, 70). Thus, MHC-I molecules bound to low affinity peptides have a shorter plasma membrane half-life, and are less likely to trigger a CD8 T cell response (71, 72). Notwithstanding, this model has been challenged by recent studies showing in vivo responses to low affinity peptide neoantigens in murine models, in discordance with in vitro peptide binding assays (73, 74). Our structural findings suggest that low-affinity peptides could in principle still associate with nascent MHC-I molecules, under chaperone assistance, so long as they have a favorable P2 anchor and interactions with conserved MHC-I residues in the A-, B-, and C- pockets. While this model remains to be validated in vivo, our results provide a plausible explanation for the observed immunogenicity of suboptimal peptides in functional T cell activation studies.

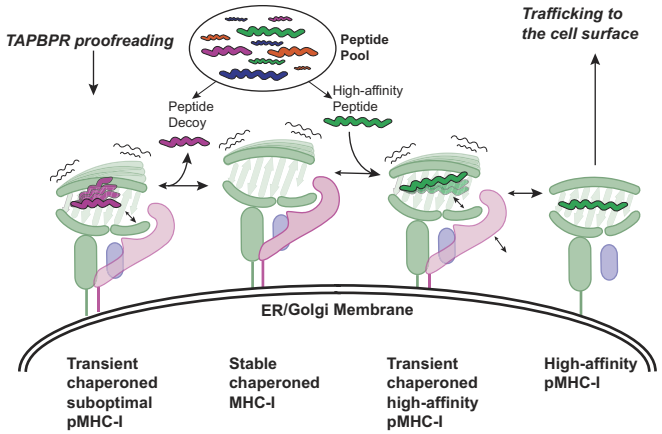

Fig. 6. Structural mechanism of peptide antigen proofreading by TAPBPR. Empty MHC-I is preferentially recognized by TAPBPR in a peptide-receptive, open conformation. Chaperoned MHC-I screens a large peptide pool in the endoplasmic reticulum through transient complexes. TABBPR widens the $\alpha_{2\text{-}1}$ helix of the peptide binding groove, enhances the dynamics of the α_1 helix, and induces an unstructured F-pocket. Thus, chaperone MHC-I exhibits a lower affinity toward incoming peptides and promotes the dissociation of suboptimal peptide decoys. When chaperoned MHC-I proofreads a high-affinity peptide, the N terminal peptide forms native-like contacts with its A- and B-pockets. The peptide C-terminus interacts with peptide-coordinating MHC-I residues in the F-pocket to stabilize the peptide binding groove in a closed conformation, which allosterically promotes the release of TAPBPR.

The TAPBPR G24-R36 loop has been previously suggested to directly mediate peptide editing by competing with the peptide C-terminus for binding to the MHC-I F-pocket (30, 42, 43). More recent studies using solution NMR have challenged this "scooping/levering" mechanism by explicitly showing that the TAPBPR loop adopts a disordered conformation, which forms hydrophobic contacts with the rim of the $\alpha_{2\text{-}1}$ helix, instead of entering the empty MHC-I groove in a solution environment (32, 38). Our engineered high-affinity TAPBPR^{HiFi} corroborates this model, by showing that the S104F mutation on the edge of the TAPBPR loop contributes to enhanced binding on peptide-loaded MHC-I molecules. In further agreement with our previous NMR studies (38) and the lack of clear electron density in the structure of both MHC-I/TAPBPR complexes (29, 30), we find that, even though the F-pocket of the MHC-I groove in complex with the heptamer peptide decoy is completely empty, electron density for the loop residues G24-R36 is completely lacking in our data, supporting a more disordered ensemble of conformations, which does not enter the MHC-I groove. Taken together, our results support that TAPBPR promotes peptide editing by perturbing the regular structure of the MHC-I F-pocket, including a widened $\alpha_{2\text{-}1}$ and a partially unfolded α_1 helix, rather than by directly competing with the peptide C terminus.

Our solution structure, biophysical and biochemical insights now provide a complete view of how TAPBPR, and by extension tapasin, can proofread the intracellular peptide pool to select an optimized repertoire of epitopes for MHC-I antigen presentation on the cell surface. The extreme polymorphism of HLAs results in a wide range of dependencies on molecular chaperones for peptide loading and repertoire optimization. It is plausible that different MHC-I molecules employ a similar proofreading mechanism to select their presented ligands irrespective of their associations with tapasin, or TAPBPR. This view aligns with biophysical studies showing that chaperones act by manipulating existing states of a relatively malleable MHC-I structure, rather than by inducing drastically new structures (22, 32). The extent to which these findings carry over to chaperone-independent peptide loading must be characterized using analogous solution experiments employing stabilized MHC-I molecules with partial ligands.

Materials and Methods

Specific details about protein expression and purification, mass spectrometry, SPR, NMR, cryoEM data processing, FP anisotropy, single-antigen HLA bead assays, and functional peptide exchange experiments in cells, are outlined in detail in *SI Appendix* (75). Briefly, recombinant peptide/MHC-I (41) and TAPBPR (32) proteins were produced using established expression protocols in *Escherichia coli* and *Drosophila* S2 cells, respectively. NMR chemical shift mapping for the TAX9/HLA-A*02:01 molecule upon binding to TAPBPR^{HiFi} was performed in an analogous fashion to TAPBPR^{WT}, described in our previous work (22). The open peptide-loaded HLA-A*02:01/TAPBPR^{HiFi} complex was obtained by mixing open HLA-A*02:02/TAX9 and TAPBPR^{HiFi} at a 1:1.3 molar ratio. The mixture was incubated at 4 °C for 1 h and followed by 40-min UV irradiation, and the complex was purified by size-exclusion chromatography. The peak fraction at 0.2 mg/mL concentration was used for grid preparation. The sample was applied to freshly plasma cleaned Quantifoil Cu 300 2/2 (Quantifoil) grids and was plunge frozen in liquid ethane using the Vitroblot Mark IV (Thermo Fisher) operated at 4 °C and 100% humidity. The dataset was collected on a Titan Krios G3i 300 kV electron microscope (Thermo Fisher Scientific) with a 20 eV energy filter and equipped with a K3 Summit camera (Gatan). Superresolution images were collected over thirty-five frames with a dose of 40.5 e − /Å^2 at a nominal magnification of x105,000, resulting in a pixel size of 0.418 Å/pixel. The defocus range was set from −0.8 to −3.0 μm. The model of the MHC-I/TAPBPR complex was built iteratively in ISOLDE (76), Coot (77), and PHENIX (78), using PDB 2VLL as the starting model. Images of the models and maps for figures were rendered using ChimeraX (79) and Pymol (80).

Data, Materials, and Software Availability. All structures and cryoEM density data associated with this study have been deposited in the PDB and EMDB, under PDB ID 9C96 and EMDB entry ID EMD-45360. NMR assignments have been deposited in the BMRB, under code 52520. All other data relating to this paper are deposited in Dryad via https://doi.org/10.5061/dryad.prr4xgxvv.

ACKNOWLEDGMENTS. We acknowledge Dr. Hoang-Anh Phan (CHOP) for assistance with mass spectrometry and Sagar Gupta for assistance with preparing movies and peptide sequence logos. We are grateful to Dr. Derin Keskin (Harvard University) for sharing the HLA monoallelic cell lines, Dr. Dimitri Monos (CHOP) for assistance with running the SAB experiments, Dr. John Maris (CHOP) for sharing the T2 cell line, and Dr. Frank DiMaio (University of Washington) for assistance with structure modeling using Rosetta. We also acknowledge the use of instruments at the Electron Microscopy Resource Lab and at the Beckman Center for Cryo-Electron Microscopy at the Institute of Structural Biology at the University of Pennsylvania Perelman School of Medicine. We thank Drs. Prerana Gogoi and Sudheer Molugu for assistance with Krios microscope operation at the University of Pennsylvania. NIH grants R01AI143997 (N.G.S.), R35GM125034 (N.G.S.), U01DK112217 (N.G.S.), R35GM144120 (V.Y.M.-B.), The Asplundh Foundation, and The Children's Hospital of Philadelphia Cell and Gene Therapy Collaborative. This work was delivered as part of the NexTGen team supported by the Cancer Grand Challenges partnership funded by Cancer Research UK (CGCATF-2021/100002) and the National Cancer Institute (CA278687-01) and The Mark Foundation for Cancer Research.

Author affiliations: [a]Department of Biochemistry and Biophysics, Perelman School of Medicine at the University of Pennsylvania, Philadelphia, PA 19104; [b]Center for Computational and Genomic Medicine and Department of Pathology and Laboratory Medicine, Children's Hospital of Philadelphia, Philadelphia, PA 19104; [c]Department of Systems Pharmacology and Translational Therapeutics, Perelman School of Medicine, University of Pennsylvania, Philadelphia, PA 19104; and [d]Immunology Graduate Program, Perelman School of Medicine at the University of Pennsylvania, Philadelphia, PA 19104

Author contributions: Y.S., V.Y.M.-B., and N.G.S. designed research; Y.S., R.A.P., L.M., A.C., C.W., D.H., J.N.D., and K.D.G. performed research; Y.S. contributed new reagents/analytic tools; Y.S. analyzed data; and Y.S. and N.G.S. wrote the paper.

1. P. Cresswell, N. Bangia, T. Dick, G. Diedrich, The nature of the MHC class I peptide loading complex. *Immunol. Rev.* **172**, 21–28 (1999).
2. P. Cresswell, A. L. Ackerman, A. Giodini, D. R. Peaper, P. A. Wearsch, Mechanisms of MHC class I-restricted antigen processing and cross-presentation. *Immunol. Rev.* **207**, 145–157 (2005), 10.1111/j.0105-2896.2005.00316.x.
3. J. S. Blum, P. A. Wearsch, P. Cresswell, Pathways of antigen processing. *Annu. Rev. Immunol.* **31**, 443–473 (2013), 10.1146/annurev-immunol-032712-095910.
4. J. Rossjohn *et al.*, T cell antigen receptor recognition of antigen-presenting molecules. *Annu. Rev. Immunol.* **33**, 169–200 (2015), 10.1146/annurev-immunol-032414-112334.
5. J. W. Yewdell, MHC class I immunopeptidome: Past, present, future. *Mol. Cell. Proteomics* **21**, 100230 (2022), 10.1016/j.mcpro.2022.100230.
6. C. A. Klebanoff *et al.*, T cell receptor therapeutics: Immunologic targeting of the intracellular cancer proteome. *Nat. Rev. Drug Discov.* **22**, 996–1017 (2023), 10.1038/s41573-023-00809-z.
7. A. Sette, J. Sidney, HLA supertypes and supermotifs: A functional perspective on HLA polymorphism. *Curr. Opin. Immunol.* **10**, 478–482 (1998), 10.1016/S0952-7915(98)80124-6.
8. J. Sidney *et al.*, HLA class I supertypes: A revised and updated classification. *BMC Immunol.* **9**, 1 (2008), 10.1186/1471-2172-9-1.
9. M. Rasmussen *et al.*, Uncovering the peptide-binding specificities of HLA-C: A general strategy to determine the specificity of any MHC class I molecule. *J. Immunol. Author Choice* **193**, 4790–4802 (2014), 10.4049/jimmunol.1401689.
10. J. C. Solheim *et al.*, Prominence of beta 2-microglobulin, class I heavy chain conformation, tapasin in the interactions of class I heavy chain with calreticulin and the transporter associated with antigen processing. *J. Immunol.* **158**, 2236–2241 (1997), 10.4049/jimmunol.158.5.2236.
11. M. Chen, M. Bouvier, Analysis of interactions in a tapasin/class I complex provides a mechanism for peptide selection. *EMBO J.* **26**, 1681–1690 (2007), 10.1038/sj.emboj.7601624.
12. M. Howarth *et al.*, Tapasin enhances MHC class I peptide presentation according to peptide half-life. *Proc. Natl. Acad. Sci.* **101**, 11737–11742 (2004), 10.1073/pnas.0306294101.
13. J. Brunnberg *et al.*, Dual role of the peptide-loading complex as proofreader and limiter of MHC-I presentation. *Proc. Natl. Acad. Sci. U.S.A.* **121**, e2321600121 (2023), 10.1073/pnas.2321600121.
14. M. S. Teng *et al.*, A human TAPBP (TAPASIN)-related gene. TAPBP-R. *Eur. J. Immunol.* **32**, 1059–1068 (2002).
15. L. H. Boyle *et al.*, Tapasin-related protein TAPBPR is an additional component of the MHC class I presentation pathway. *Proc. Natl. Acad. Sci.* **110**, 3465–3470 (2013), 10.1073/pnas.1222342110.
16. T. Elliott, A. Williams, The optimization of peptide cargo bound to MHC class I molecules by the peptide-loading complex. *Immunol. Rev.* **207**, 89–99 (2005), 10.1111/j.0105-2896.2005.00311.x.
17. J. Jiang *et al.*, Chaperone-mediated MHC-I peptide exchange in antigen presentation. *IUCrJ* **11**, 287–298 (2024), 10.1107/S2052252524002768.
18. F. T. Ilca *et al.*, Distinct polymorphisms in HLA class I molecules govern their susceptibility to peptide editing by TAPBPR. *Cell Rep.* **29**, 1621–1632.e3 (2019), 10.1016/j.celrep.2019.09.074.
19. Y. Sun *et al.*, Xeno interactions between MHC-I proteins and molecular chaperones enable ligand exchange on a broad repertoire of HLA allotypes. *Sci. Adv.* **9**, eade7151 (2023), 10.1126/sciadv.ade7151.
20. A. A. Bashirova *et al.*, HLA tapasin independence: Broader peptide repertoire and HIV control. *Proc. Natl. Acad. Sci.* **117**, 28232–28238 (2020), 10.1073/pnas.2013554117.
21. M. Raghavan, J. Geng, HLA-B polymorphisms and intracellular assembly modes. *Mol. Immunol.* **68**, 89–93 (2015), 10.1016/j.molimm.2015.07.007.
22. A. C. McShan *et al.*, Molecular determinants of chaperone interactions on MHC-I for folding and antigen repertoire selection. *Proc. Natl. Acad. Sci.* **116**, 25602–25613 (2019), 10.1073/pnas.1915562116.
23. A. C. McShan *et al.*, TAPBPR employs a ligand-independent docking mechanism to chaperone MR1 molecules. *Nat. Chem. Biol.* **18**, 859–868 (2022), 10.1038/s41589-022-01049-9.
24. H. E. G. McWilliam *et al.*, Endoplasmic reticulum chaperones stabilize ligand-receptive MR1 molecules for efficient presentation of metabolite antigens. *Proc. Natl. Acad. Sci.* **117**, 24974–24985 (2020), 10.1073/pnas.2011260117.
25. C. A. Kulicke *et al.*, Delivery of loaded MR1 monomer results in efficient ligand exchange to host MR1 and subsequent MR1T cell activation. *Commun. Biol.* **7**, 1–13 (2024), 10.1038/s42003-024-05912-4.
26. S. A. Overall *et al.*, High throughput pMHC-I tetramer library production using chaperone-mediated peptide exchange. *Nat. Commun.* **11**, 1909 (2020), 10.1038/s41467-020-15710-1.
27. F. T. Ilca *et al.*, Utilizing TAPBPR to promote exogenous peptide loading onto cell surface MHC I molecules. *Proc. Natl. Acad. Sci. U.S.A.* **115**, E9353–E9361 (2018), 10.1073/pnas.1809465115.
28. S. M. O'Rourke, G. I. Morozov, J. T. Roberts, A. W. Barb, N. G. Sgourakis, Production of soluble pMHC-I molecules in mammalian cells using the molecular chaperone TAPBPR. *Protein Eng. Des. Sel.* **32**, 525–532 (2019). https://doi.org/10.1093/protein/gzaa015.
29. J. Jiang *et al.*, Crystal structure of a TAPBPR-MHC I complex reveals the mechanism of peptide editing in antigen presentation. *Science* **358**, 1064–1068 (2017), 10.1126/science.aao5154.
30. C. Thomas, R. Tampé, Structure of the TAPBPR–MHC I complex defines the mechanism of peptide loading and editing. *Science* **358**, 1060–1064 (2017), 10.1126/science.aao6001.
31. G. Dong *et al.*, Insights into MHC class I peptide loading from the structure of the tapasin/ERp57 heterodimer. *Immunity* **30**, 21–32 (2009), 10.1016/j.immuni.2008.10.018.
32. A. C. McShan *et al.*, Peptide exchange on MHC-I by TAPBPR is driven by a negative allostery release cycle. *Nat. Chem. Biol.* **14**, 811–820 (2018), 10.1038/s41589-018-0096-2.
33. I. K. Müller *et al.*, Structure of an MHC I–tapasin–ERp57 editing complex defines chaperone promiscuity. *Nat. Commun.* **13**, 5383 (2022), 10.1038/s41467-022-32841-9.
34. J. Jiang *et al.*, Structural mechanism of tapasin-mediated MHC-I peptide loading in antigen presentation. *Nat. Commun.* **13**, 5470 (2022), 10.1038/s41467-022-33153-8.
35. A. Domnick *et al.*, Molecular basis of MHC I quality control in the peptide loading complex. *Nat. Commun.* **13**, Article ID 4701, (2022). https://doi.org/10.1038/s41467-022-32384-z.
36. A. Blees *et al.*, Structure of the human MHC-I peptide-loading complex. *Nature* **551**, 525–528 (2017). https://doi.org/10.1038/nature24627.
37. G. I. Morozov *et al.*, Interaction of TAPBPR, a tapasin homolog, with MHC-I molecules promotes peptide editing. *Proc. Natl. Acad. Sci. U.S.A.* **113**, E1006–E1015 (2016), 10.1073/pnas.1519894113.
38. A. C. McShan *et al.*, TAPBPR promotes antigen loading on MHC-I molecules using a peptide trap. *Nat. Commun.* **12**, 3174 (2021), 10.1038/s41467-021-23225-6.
39. R. Satti *et al.*, Get into the groove! The influence of TAPBPR on cargo selection. *Curr. Opin. Immunol.* **83**, 102346 (2023), 10.1016/j.coi.2023.102346.
40. D. H. Margulies *et al.*, Chaperone function in antigen presentation by MHC class I molecules–tapasin in the PLC and TAPBPR beyond. *Front. Immunol.* **14**, 1179846 (2023), 10.3389/fimmu.2023.1179846.
41. Y. Sun *et al.*, Universal open MHC-I molecules for rapid peptide loading and enhanced complex stability across HLA allotypes. *Proc. Natl. Acad. Sci.* **120**, e2304055120 (2023), 10.1073/pnas.2304055120.
42. L. Sagert *et al.*, A loop structure allows TAPBPR to exert its dual function as MHC I chaperone and peptide editor. *eLife* **9**, e55326 (2020), 10.7554/eLife.55326.
43. F. T. Ilca *et al.*, TAPBPR mediates peptide dissociation from MHC class I using a leucine lever. *eLife* **7**, e40126 (2018), 10.7554/eLife.40126.
44. C. Hermann *et al.* TAPBPR and tapasin binding to MHC class I is mutually exclusive. *J. Immunol. Baltim. Md 1950* **191**, 1300929 (2013), 10.4049/jimmunol.1300929.
45. Y. Song *et al.*, High resolution comparative modeling with RosettaCM. *Struct. Lond. Engl.* **1993**, 21 (2013), 10.1016/j.str.2013.08.005.
46. G. F. Papadaki *et al.*, A chicken tapasin ortholog can chaperone empty HLA-B∗37:01 molecules independent of other peptide-loading components. *J. Biol. Chem.* **299**, 105136 (2023), 10.1016/j.jbc.2023.105136.
47. Y. Sun *et al.*, Structural principles of peptide-centric chimeric antigen receptor recognition guide therapeutic expansion. *Sci. Immunol.* **8**, eadj5792 (2023). https://doi.org/10.1126/sciimmunol.adj5792.
48. A. Chaudhuri, N. Sgourakis, Data_52520. The Biological Magnetic Resonance Data Bank. https://bmrb.io/author_view/52520_hy_jjbshxwx.str. Deposited 23 July 2024.
49. M. Toebes *et al.*, Design and use of conditional MHC class I ligands. *Nat. Med.* **12**, 246–251 (2006), 10.1038/nm1360.
50. A. H. Bakker *et al.*, Conditional MHC class I ligands and peptide exchange technology for the human MHC gene products HLA-A1, -A3, -A11, and -B7. *Proc. Natl. Acad. Sci. U.S.A.* **105**, 3825–3830 (2008), 10.1073/pnas.0709717105.
51. J. Ishizuka *et al.*, The structural dynamics and energetics of an immunodominant T cell receptor are programmed by its Vβ domain. *Immunity* **28**, 171–182 (2008), 10.1016/j.immuni.2007.12.018.
52. R. P. Pumroy, L. Mallik, Y. Sun, Y. V. Moiseenkova-Bell, N. Sgourakis, 9C96. The Protein Data Bank. http://www.rcsb.org/pdb/explore/explore.do?structureId=9C96. Deposited 17 June 2024.
53. R. P. Pumroy, L. Mallik, Y. Sun, Y. V. Moiseenkova-Bell, N. Sgourakis, EMD-45360. The Electron Microscopy Data Bank. https://www.ebi.ac.uk/emdb/EMD-45360. Deposited 17 June 2024.
54. A. T. Nguyen *et al.*, The pockets guide to HLA class I molecules. *Biochem. Soc. Trans.* **49**, 2319–2331 (2021), 10.1042/BST20210410.

55. P. H. N. Celie *et al.*, UV-induced ligand exchange in MHC class I protein crystals. *J. Am. Chem. Soc.* **131**, 12298–12304 (2009), 10.1021/ja9037559.
56. A. C. McShan *et al.*, Conformational plasticity of RAS Q61 family of neoepitopes results in distinct features for targeted recognition. *Nat. Commun.* **14**, 8204 (2023), 10.1038/s41467-023-43654-9.
57. A. van Hateren *et al.*, Direct evidence for conformational dynamics in major histocompatibility complex class I molecules. *J. Biol. Chem.* **292**, 20255–20269 (2017), 10.1074/jbc.M117.809624.
58. P. A. Reche *et al.*, Elicitation from virus-naive individuals of cytotoxic T lymphocytes directed against conserved HIV-1 epitopes. *Med. Immunol.* **5**, 1 (2006), 10.1186/1476-9433-5-1.
59. R. D. Salter, P. Cresswell, Impaired assembly and transport of HLA-A and -B antigens in a mutant TxB cell hybrid. *EMBO J.* **5**, 943 (1986), 10.1002/j.1460-2075.1986.tb04307.x.
60. A. Steinle, D. J. Schendel, HLA class I alleles of LCL 721 and 174XCEM.T2 (T2). *Tissue Antigens* **44**, 268–270 (1994), 10.1111/j.1399-0039.1994.tb02394.x.
61. R. Abele, R. Tampé, Moving the cellular peptidome by transporters. *Front. Cell Dev. Biol.* **6**, 43 (2018), 10.3389/fcell.2018.00043.
62. A. Aflalo, L. H. Boyle, Polymorphisms in MHC class I molecules influence their interactions with components of the antigen processing and presentation pathway. *Int. J. Immunogenet.* **48**, 317–325 (2021), 10.1111/iji.12546.
63. P. A. Wearsch, P. Cresswell, The quality control of MHC class I peptide loading. *Curr. Opin. Cell Biol.* **20**, 624–631 (2008), 10.1016/j.ceb.2008.09.005.
64. D. H. Margulies *et al.*, Chaperones and catalysts: How antigen presentation pathways cope with biological necessity. *Front. Immunol.* **13**, 859782 (2022).
65. D. H. Margulies *et al.*, "Structure and function of molecular chaperones that govern immune peptide loading" in *Macromolecular Protein Complexes II: Structure and Function Subcellular Biochemistry*, J. R. Harris, J. Marles-Wright, Eds. (Springer International Publishing, 2019), pp. 321–337. 10.1007/978-3-030-28151-9_10.
66. L. Li *et al.*, Crystal structures of MHC class I complexes reveal the elusive intermediate conformations explored during peptide editing. *Nat. Commun.* **14**, 5020 (2023), 10.1038/s41467-023-40736-6.
67. P. H. N. Celie *et al.*, UV-induced ligand exchange in MHC class I protein crystals. *J. Am. Chem. Soc.* **131**, 12298–12304 (2009), 10.1021/ja9037559.
68. H. Lan *et al.*, Exchange catalysis by tapasin exploits conserved and allele-specific features of MHC-I molecules. *Nat. Commun.* **12**, 4236 (2021), 10.1038/s41467-021-24401-4.
69. C. Dirscherl *et al.*, Dissociation of β2m from MHC class I triggers formation of noncovalent transient heavy chain dimers. *J. Cell Sci.* **135**, jcs259489 (2022), 10.1242/jcs.259498.
70. F. M. Ruggiero, S. Springer, Homotypic and heterotypic in cis associations of MHC class I molecules at the cell surface. *Curr. Res. Immunol.* **3**, 85–99 (2022), 10.1016/j.crimmu.2022.05.001.
71. G. B. Zagorac *et al.*, Early endosomal rerouting of major histocompatibility class I conformers. *J. Cell. Physiol.* **227**, 2953–2964 (2012), 10.1002/jcp.23042.
72. E. Olson, M. Raghavan, Major histocompatibility complex class I assembly within endolysosomal pathways. *Curr. Opin. Immunol.* **84**, 102356 (2023), 10.1016/j.coi.2023.102356.
73. M. A. Gillig *et al.*, CD8+ T cell-dependent antitumor activity in vivo of a mass spectrometry-identified neoepitope despite undetectable CD8+ immunogenicity in vitro. *J. Immunol. Baltim. Md* **1950**, 1783–1791 (2023), 10.4049/jimmunol.2300356.
74. H. Ebrahimi-Nik *et al.*, Reversion analysis reveals the in vivo immunogenicity of a poorly MHC I-binding cancer neoepitope. *Nat. Commun.* **12**, 6423 (2021), 10.1038/s41467-021-26646-5.
75. N. Sgourakis, doi:10.5061/dryad.prr4xgxvv. Dryad. https://doi.org/10.5061/dryad.prr4xgxvv. Deposited 25 June 2024.
76. T. I. Croll, ISOLDE: A physically realistic environment for model building into low-resolution electron-density maps. *Acta Crystallogr. Sect. Struct. Biol.* **74**, 519–530 (2018), 10.1107/S2059798318002425.
77. P. Emsley, K. Cowtan, Coot: Model-building tools for molecular graphics. *Acta Crystallogr. D Biol. Crystallogr.* **60**, 2126–2132 (2004), 10.1107/S0907444904019158.
78. P. V. Afonine *et al.*, Real-space refinement in PHENIX for cryo-EM and crystallography. *Acta Crystallogr. Sect. Struct. Biol.* **74**, 531–544 (2018), 10.1107/S2059798318006551.
79. T. D. Goddard *et al.*, UCSF ChimeraX: Meeting modern challenges in visualization and analysis. *Protein Sci.* **27**, 14–25 (2018), 10.1002/pro.3235.
80. Schrödinger LLC, *The PyMOL Molecular Graphics System, Version 1.8* (2015).